Structure of the Two Transmembrane Cu$^+$ Transport Sites of the Cu$^+$-ATPases*[S]

Manuel González-Guerrero[‡1], Elif Eren[‡1,2], Swati Rawat[§], Timothy L. Stemmler[§], and José M. Argüello[‡3]

From the ‡Department of Chemistry and Biochemistry, Worcester Polytechnic Institute, Worcester, Massachusetts 01609 and the §Department of Biochemistry and Molecular Biology, Wayne State University School of Medicine, Detroit, Michigan 48201

Cu$^+$-ATPases drive metal efflux from the cell cytoplasm. Paramount to this function is the binding of Cu$^+$ within the transmembrane region and its coupled translocation across the permeability barrier. Here, we describe the two transmembrane Cu$^+$ transport sites present in *Archaeoglobus fulgidus* CopA. Both sites can be independently loaded with Cu$^+$. However, their simultaneous occupation is associated with enzyme turnover. Site I is constituted by two Cys in transmembrane segment (TM) 6 and a Tyr in TM7. An Asn in TM7 and Met and Ser in TM8 form Site II. Single site x-ray spectroscopic analysis indicates a trigonal coordination in both sites. This architecture is distinct from that observed in Cu$^+$-trafficking chaperones and classical cuproteins. The high affinity of these sites for Cu$^+$ (Site I K_a = 1.3 fm^{-1}, Site II K_a = 1.1 fm^{-1}), in conjunction with reversible direct Cu$^+$ transfer from chaperones, points to a transport mechanism where backward release of free Cu$^+$ to the cytoplasm is largely prevented.

Copper is an essential micronutrient (1, 2). It has critical catalytic and electron transfer roles in a number of key proteins (tyrosinase, lysyl oxidase, ferroxidase ceruloplasmin, plastocyanin, etc.). However, when free, copper participates in the production of reactive oxygen species leading to cellular damage. Toward sustaining intracellular copper balance, transmembrane transport systems maintain the copper cell quota, Cu$^+$ chaperone proteins traffic the bound metal to specific cellular targets, and metal-sensing transcription factors control copper dependent protein expression (3–5). The metal coordination geometry in these proteins is central to the efficiency of the Cu$^+$

mobilization processes. In this direction, the coordination should ensure the specificity and prevent the release of free Cu$^+$ to the cytoplasm. Canonical copper metalloproteins have long been characterized and classified based on spectroscopic and magnetic properties (Types I, II, and III) (6–8). Their study has provided great detail on copper coordination in "permanent" sites where copper is bound during the functional life of the proteins. Cu$^+$ linear coordination by invariant Cys residues of chaperone proteins has been described, providing insight into the mechanism of copper trafficking and exchange among similar domains (9, 10). More recently, trigonal coordination by Cys$_2$-His sites has been observed, for instance, in *Mycobacterium tuberculosis* transcription factor CsoR (11). Alternatively, Met$_n$His was found in several Cu$^+$-trafficking proteins located in the oxidizing periplasm of prokaryotes (12–14). Despite this progress, Cu$^+$ distribution and balance cannot be understood without describing the selective coordination during compartmental transmembrane transport.

In eukaryotic cells, members of the Ctr family of proteins transport Cu$^+$ inside the cell (15). Ctr1 organizes as homotrimers forming transmembrane pores that facilitate Cu$^+$ transmembrane translocation by an apparently energy-independent undefined mechanism (16, 17). Although relevant Cu$^+$-binding Met have been observed in the extracellular loops of Ctr1 (15); none of the invariant transmembrane residues appear to be required for transport, and no direct coordination is evident (17).

As a counterpart to influx systems, Cu$^+$-ATPases are responsible for cytoplasmic Cu$^+$ efflux. Mutations of the human Cu$^+$-ATPase genes, ATP7A and ATP7B, lead to Menkes syndrome and Wilson disease, respectively (18, 19). Cu$^+$-ATPases are members of the superfamily of P-type ATPases (20, 21). These couple Cu$^+$ transport to the hydrolysis of ATP, following a classical Post catalytic/transport cycle (19, 21). In this mechanism, transmembrane metal-binding sites (TM-MBSs)[4] are responsible for handling the ion during transmembrane translocation (22). These transmembrane sites are exposed to the cytoplasm when they receive the ion from the partnering Cu$^+$ chaperone (23). Upon enzyme phosphorylation (formation of E1P intermediary), Cu$^+$ is transiently occluded within the transmembrane region. The transported metal is released following the opening of the TM-MBS to the extracellular (vesicular/luminal) compartment (E2P intermedi-

[4] The abbreviations used are: TM, transmembrane segment; MBS, metal-binding site; EXAFS, extended x-ray absorption fine structure; XANES, x-ray absorption near edge structure.

ary). Because of the coupled nature of this mechanism, *i.e.* Cu$^+$ transport is tied to ATP hydrolysis, the stoichiometry of transport and the associated energy requirements are linked to the number and structure of TM-MBSs. Cu$^+$-ATPases consist of eight transmembrane segments (TM), two large cytosolic loops comprising the actuator, phosphorylation and nucleotide-binding domains, and regulatory metal-binding domains in their N terminus (exceptionally in the C terminus) (20, 21, 24 –27). Analysis of Cu$^+$-ATPase TM sequences revealed the presence of only six invariant residues, two Cys in the sixth TM (H6), Asn and Tyr in the seventh TM (H7), and Met and Ser residues in the eighth TM (H8) (24). Subsequent mutagenesis studies of *Archaeoglobus fulgidus* CopA, a model Cu$^+$-ATPase, showed that these residues are required for completion of the Cu$^+$-dependent steps in the ATPase catalytic/transport cycle (22).

In this work, we describe the Cu$^+$ coordination during transport by Cu$^+$-ATPases. The invariant transmembrane amino acids form two Cu$^+$-binding sites through trigonal coordination. The structures and characteristics of these sites support a model mechanism for the direct metal exchange with Cu$^+$ chaperones while ensuring the unfeasibility of Cu$^+$ ion release to the cytoplasm.

EXPERIMENTAL PROCEDURES

Site-directed Mutagenesis and Protein Expression—Preparation of wild type CopA, C27A,C30A,C751A,C754A CopA (C$_2$-CopA) and C27A,C30A,C380A,C382A,C751A,C754A CopA (C$_0$-CopA) cDNAs cloned into the pCRT7/NT-TOPO/His vector (Invitrogen) have been described (28). Mutations C380A, C382A, Y682A, N683A, M711A, and S715A were introduced in both C$_2$-CopA and C$_0$-CopA backgrounds using the QuikChange™ site-directed mutagenesis kit (Stratagene, La Jolla, CA). The mutations were confirmed by DNA sequencing (MacrogenUSA, Rockville, MD). A streptavidin tag was introduced to the C terminus of CopA, C$_2$-CopA, and C$_0$-CopA by amplifying the coding cDNAs in the pCRT7/NT-TOPO/His vector (Invitrogen) using primer 5′-AGCGCTTGGAGCCAC-CCGCAGTTCGAAAAATAAAAGGGCGAATTCGAAGC-TTGA and the complementary 3′ primer. The resulting amplicons were transformed into *Escherichia coli* BL21(DE3)pLysS cells (Invitrogen). Subsequently the His tags still encoded by these constructs were removed by amplification with primer 5′-TAAGACGATGACGATAAGGATAGGAGGCCAACCC-TTATG and complementary 3′. These primers introduced a stop codon after the His coding sequence and placed a second ribosome-binding site (AGGAGG) prior to the ATG codon of the proteins. All of the constructs were introduced into BL21(DE3)pLysS *E. coli* cells (Invitrogen), and expression was induced with 0.75 mM isopropyl β-D-thiogalactopyranoside for 3 h.

Enzyme Preparation—His-tagged proteins were prepared as previously described (29). Streptavidin-tagged proteins were solubilized in a similar manner. After membrane solubilization, dodecyl-β-D-maltoside was removed by addition of Bio-Beads SM-2 (Bio-Rad), and protein purification was performed using streptavidin tag affinity chromatography as previously described (30). Purified proteins were stored in 50 mM HEPES, 200 mM NaCl, 10 mM ascorbic acid, pH 7.5, at −80 °C. Protein concentration determinations were performed in accordance to Bradford (31) using bovine serum albumin as a standard. The accuracy of colorimetric protein measurements was confirmed by total amino acid analysis (Keck Facility, Yale University, New Haven, CT).

p-Nitrophenyl Phosphatase Assays—*p*-Nitrophenyl phosphatase activity determinations were performed as described (32).

Determination of Cu$^+$ Binding Stoichiometry and Affinity—Cu$^+$ binding determinations were carried out in a buffer containing: 50 mM HEPES, pH 7.5, 200 mM NaCl, 0.01% dodecyl-β-D-maltoside, 0.01% asolectin, 10 mM ascorbic acid, 100 μM CuSO$_4$, and 10 μM protein. When indicated 2 mM ATP, 0.2 mM Na$_3$VO$_4$, 0.1 mM AlF$_4^-$ or 0.2 mM LaCl$_3$, and 2 mM ATP were included in the media together with 5 mM MgCl$_2$. The system was allowed to reach equilibrium for 5 min at room temperature, and excess Cu$^+$ was removed using a Sephadex-G25 column (Sigma). Following precipitation of proteins with 10% trichloroacetic acid, Cu$^+$ was determined by BCA assay as described (33). Cu$^+$ binding affinities were determined by metal titrations of wild type or mutated proteins in the presence of BCA (23, 34). 10 μM protein and 25 μM BCA were titrated with 1–125 μM Cu$^+$ in a buffer containing: 50 mM HEPES, pH 7.5, 200 mM NaCl, 0.01% dodecyl-β-D-maltoside, 0.01% asolectin, and 10 mM ascorbic acid, and the absorbance change between 330 nm and 410 nm was monitored. Protein absorbance was subtracted from the data. Free metal concentrations were calculated from $K_{BCA} = [BCA_2Cu]/[BCA_{free}]^2[Cu^+]$, where K_{BCA} is the association constant of BCA for Cu. An extinction coefficient of 43000 M^{-1} cm^{-1} at 359 nm for Cu$^+$ bound BCA and K_{BCA} of 4.6×10^{14} M^{-2} for Cu$^+$ was used in determinations of free Cu$^+$ concentration (23, 34). The Cu$^+$-protein K_a and the number of metal-binding sites (n) were calculated from $\nu = n[Cu^+]_f K_a/(1+K_a[Cu^+]_f)$, where ν is the molar ratio of Cu$^+$ bound to protein. Reported errors for K_a and n are asymptotic standard errors provided by the fitting software (Origin, OriginLab, Northampton, MA). The plotted data points are the means ± S.E. of at least three experiments performed with independent protein preparations.

XAS Analysis—Protein samples were fully loaded with Cu$^+$ as described above and concentrated to 0.5 mM. XAS data were collected at the Stanford Synchrotron Radiation Laboratory on beamline 9-3, using a Si(220) double crystal monochromator equipped with a harmonic rejection mirror. The samples were maintained at 10 K using Oxford Instruments continuous-flow liquid helium cryostat. Protein fluorescence excitation spectra were collected using a 30-element Ge solid state array detector. A nickel filter (0.6 μM in width) and solar slits were placed between the cryostat and detector to filter scattering fluorescence not associated with protein copper signals. XAS spectra were measured using 5-eV steps in the pre-edge region (8750 – 8960 eV), 0.25 eV steps in the edge region (8986 –9050 eV), and 0.05 Å^{-1} increments in the extended x-ray absorption fine structure (EXAFS) region (to $k = 13.5$ Å^{-1}), integrating from 1 s to 20 s in a k^3 weighted manner for a total scan length of ~40 min. X-ray energies in the protein spectra were calibrated by collecting simultaneous copper foil absorption spectra, assign-

TABLE 1

Determination of Cu$^+$ binding stoichiometry to wild type and modified CopA proteins

The values are the means $\pm$ S.E. ($n = 3$).

		Cu$^+$ bound/protein molar ratio			
		2 mM ATP	0.2 mM VO$_4^{-3}$	0.1 mM AlF$_4^-$	0.2 mM La^{+3}·ATP
CopA[a]	4.00 ± 0.30	2.29 ± 0.20	2.07 ± 0.13		3.87 ± 0.14
C$_2$-Cop[a]	1.83 ± 0.21	0.00 ± 0.03	0.00 ± 0.01	0.24 ± 0.50	2.16 ± 0.53
CopA[b]	3.94 ± 0.60				
C$_2$-CopA[b]	2.21 ± 0.07				

[a] Proteins containing a His$_6$ tag.
[b] Proteins containing a streptavidin tag.

ing the first inflection point in the foil spectra as 8980.3 eV. Every fluorescence channel of each scan was examined for spectral anomalies prior to averaging, and the spectra were closely monitored for photodamage. The data represent the averages of six to seven scans.

XAS data were processed using the Macintosh OS X version of the EXAFSPAK program suite[5] integrated with the Feff v7 software (36) for theoretical model generation. Data reduction followed a previously published protocol for a spectral resolution in bond lengths of 0.13 Å (37). EXAFS fitting analysis was performed on raw/unfiltered data. Protein EXAFS data were fit using single scattering Feff v7 theoretical models, calculated for carbon, oxygen, sulfur, and copper coordination to simulate copper-ligand environments, with values for the scale factors (Sc) and E$_0$ calibrated by fitting crystallographically characterized copper model compounds, as previously outlined (37). Criteria for judging the best fit EXAFS simulations utilized both the lowest mean square deviation between data and fit corrected for the number of degrees of freedom (F') (38) and reasonable Debye-Waller factors ($\sigma^2 < 0.006$ Å^2).

RESULTS

Identification of Transmembrane Cu$^+$-binding Sites in Cu$^+$-ATPases—Characterization of Cu$^+$-ATPase TM-MBSs required the isolation of a metal-bound form of the enzyme. Toward this goal, *A. fulgidus* CopA, a well characterized Cu$^+$-ATPase, was obtained pure in a soluble (miscellar) largely monomeric form (21, 22, 25, 26, 28, 29, 32, 39). In initial experiments, the protein was incubated at room temperature in the presence of Cu$^+$, and subsequently the free metal was removed by passage through a short Sephadex column. Four Cu$^+$ ions were bound per CopA molecule (Table 1). Because CopA has two regulatory metal-binding domains able to bind Cu$^+$ with high affinity, two of the bound Cu$^+$ were associated with these domains (23). Metal binding to cytoplasmic metal-binding domains was removed by mutation of their Cu$^+$-coordinating Cys. The resulting C27A,C30A,C751A,C754A CopA (C$_2$-CopA) construct retained only the two Cys, Cys^{380} and Cys^{382}, in H6. C$_2$-CopA was able to bind two Cu$^+$ per CopA molecule, suggesting the presence of two Cu$^+$ sites in the transmembrane region (Table 1). A number of controls were performed to verify the association of these sites with transmembrane Cu$^+$ transport. Streptavidin-tagged CopAs showed the same Cu$^+$ binding as the initially tested His$_6$-tagged constructs (Table 1). Identical results were obtained with proteins where the His$_6$ tag was enzymatically cleaved. Determinations per-

formed at high ionic strength (up to 1 M NaCl) yielded equal binding stoichiometry supporting a specific, high affinity Cu$^+$ binding. Following these findings, it was relevant to establish the association of the sites still present in C$_2$-CopA with Cu$^+$ translocation. Conclusive evidence was obtained from Cu$^+$-binding determinations performed in the presence of various ATPase ligands. The described result indicated that CopA TM-MBSs bind Cu$^+$ with a very small k_{off} that allows E1·Cu$_2^+$ separation by a relatively slow passage through a Sephadex column. However, in the presence of Mg^{2+}-ATP and Cu$^+$, the enzyme turns over, even at room temperature (where the turnover of the thermophilic CopA is minimal), and the transported ions are only transiently bound (28, 29). That is, under these conditions Cu$^+$ bound to transport sites would not remain bound during the passage through the Sephadex column, whereas ions not participating in catalysis/transport would stay bound to the protein. As expected, in the presence of Mg^{2+}-ATP the wild type CopA was eluted with two Cu$^+$ bound (to the metal-binding domains), whereas C$_2$-CopA was unable to retain the metal, indicating the likely participation of both transmembrane Cu$^+$ sites in transport (Table 1). Cu$^+$ binding measurements in the presence of VO$_4^{-3}$ or AlF$_4^-$ provided further support to this observation. These two inhibitors lock P-type ATPases in states analogous to the E2P conformation where Cu$^+$ TM-MBS should not be accessible (29, 40). As expected, in the presence of VO$_4^{-3}$ or AlF$_4^-$, CopA bound two Cu$^+$, and C$_2$-CopA was unable to bind the metal (Table 1).

Having established the catalytic binding of at least two Cu$^+$ ions, it was relevant to test the possible presence of additional transport sites. These hypothetical sites might have a lower affinity leading to metal dissociation during the relatively slow passage through the Sephadex column. In the case of the Na$^+$,K$^+$-ATPase and the Ca^{2+}-ATPase, because of the reversible nature of ion binding to these enzymes, the metal-bound (occluded) forms occurring during catalysis can only be isolated by locking the enzymes in non-turnover conditions (low temperature, presence of inhibitors, etc.) and fast separation of free and protein bound substrates (41–43). Although CopA is a thermophilic protein with very slow turnover at room temperature (28, 29), stabilization of metal bound enzyme was ensured by measuring Cu$^+$ binding in the presence of Lanthanum-ATP. This inhibitor of P-type ATPases appears to lock these enzymes in cation occluded conformations (42, 44). Lanthanum-ATP is able to inhibit CopA with a K_i of 20 μM (supplemental "Materials and Methods" and supplemental Fig. S1). In the case of CopA, no additional Cu$^+$ binding was detected in the presence of Lanthanum-ATP (Table 1), reinforcing the concept that only two Cu$^+$ TM-MBSs are involved in transport.

---

[5] G. N. George, S. J. George, and I. J. Pickering, unpublished data.

TABLE 2

Determination of *p*-nitrophenyl phosphatase activity and Cu$^+$ binding stoichiometry to modified CopA proteins

The values are the means $\pm$ S.E. ($n = 3$).

	Cu$^+$ bound/protein	*p*-Nitrophenyl phosphatase activity
		μmol/mg/min
CopA	4.00 ± 0.30	2.07 ± 0.43
CopA + 0.2 mM La^{+3}-ATP	2.16 ± 0.53	-0.05 ± 0.07
CopA + 0.1 mM AlF$_4^-$	0.24 ± 0.50	0.05 ± 0.07
C$_2$-CopA	1.83 ± 0.21	1.75 ± 0.13
C$_0$-CopA	0.97 ± 0.04	1.83 ± 0.22
C380A C$_2$-CopA	1.10 ± 0.06	1.59 ± 0.17
C382A C$_2$-CopA	1.23 ± 0.10	1.48 ± 0.12
Y682A C$_2$-CopA	0.98 ± 0.13	1.45 ± 0.18
N683A C$_2$-CopA	1.12 ± 0.02	1.48 ± 0.15
M711A C$_2$-CopA	0.92 ± 0.06	1.55 ± 0.14
S715A C$_2$-CopA	0.94 ± 0.30	1.55 ± 0.11
Y682A C$_0$-CopA	1.25 ± 0.63	1.43 ± 0.19
N683A C$_0$-CopA	0.00 ± 0.01	1.50 ± 0.07
M711A C$_0$-CopA	0.00 ± 0.01	1.48 ± 0.10
S715A C$_0$-CopA	0.08 ± 0.10	1.43 ± 0.16
C380A,M711A C$_2$-CopA	0.00 ± 0.01	1.61 ± 0.28
C380A,S715A C$_2$-CopA	0.00 ± 0.01	1.49 ± 0.01
C382A,M711A C$_2$-CopA	0.00 ± 0.01	1.70 ± 0.47
C382A,S715A C$_2$-CopA	0.00 ± 0.01	1.51 ± 0.27

FIGURE 1. **XANES spectra for C$_0$-CopA (*A*), M711A C$_2$-CopA (*B*), and C$_2$-CopA (*C*).** The spectra were offset for clarity. The *dashed vertical line* at ~8983 eV identifies spectral features corresponding to the Cu(I) 1s → 4p transition.

Cu$^+$-ATPases contain six invariant amino acids in the transmembrane region: two Cys in H6, Tyr and Asn in H7, and Met and Ser in H8 (24). Proteins carrying mutations in these residues are unable to perform Cu$^+$-dependent partial reactions (22). To ascertain their participation in the observed Cu$^+$ TM-MBSs, individual mutations of these residues were introduced into the C$_2$-CopA background. Proper folding of the resulting proteins was verified by measuring their Cu$^+$-independent *p*-nitrophenyl phosphatase activity (Table 2). Previous studies have shown this activity in *A. fulgidus* CopA (32). Furthermore, inhibition by Lanthanum-ATP and AlF$_4^-$ indicated the specificity of this assay. These proteins carrying mutations of conserved transmembrane residues were all able to bind one Cu$^+$ per molecule (Table 2), suggesting the participation of the replaced side chain in one of the two Cu$^+$ TM-MBSs. Combination of these mutations provided a better description of each site. Replacement of C380A and C382A within the C$_2$-CopA background yielded a Cys-less CopA (C$_0$-CopA). This protein was still able to bind one Cu$^+$, as did the Y682A C$_0$-CopA construct (Table 2). Alternatively, mutations N683A, M711A, and S715A in the C$_0$-CopA background removed Cu$^+$ binding. Explaining these results, a simple model can be postulated where Cys^{380}, Cys^{382}, and Tyr^{683} form one TM-MBS (Site I), whereas Asn^{683}, Met^{711}, and Ser^{715} constitute the other (Site II). Participation of both transmembrane cysteines in a single site was unexpected considering previous reports hinting distinct roles for each cysteine (45). Toward further verifying the identity of both sites, mutants were constructed where replacement of each transmembrane cysteine was combined with single mutations in Site II (Table 2). Supporting the proposed model, none of these proteins lacking a coordinating ligand in each site was able to bind Cu$^+$.

Structure of Cu$^+$ Transport Sites—The ability of mutant proteins to bind a single Cu$^+$ at either site allowed us to further explore the geometry of these sites using x-ray absorption spectroscopy. X-ray absorption near edge structure (XANES) analysis of Cu$^+$-loaded C$_2$-CopA (Sites I and II present), M711A
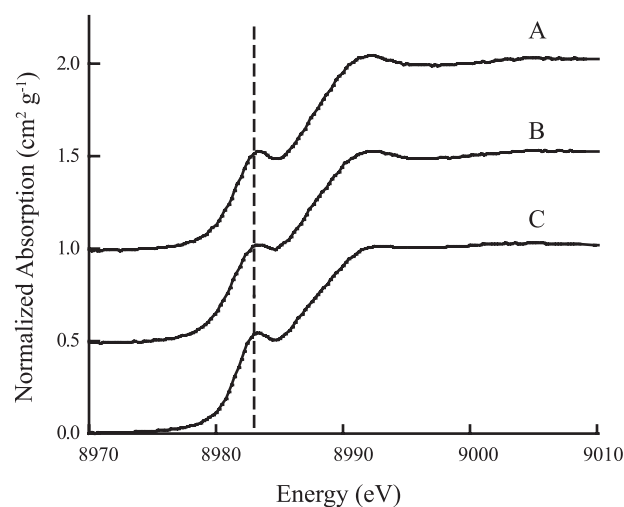
C$_2$-CopA (Site I), and C$_0$-CopA (Site II) proteins was in all cases consistent with copper coordination environments constructed by a three coordinate Cu(I)-ligand environment. XANES spectra for all three samples show pronounced pre-edge features centered at ~8984 eV (Fig. 1), consistent with Cu(I) 1s → 4p excitation signals typically observed for three coordinate cuprous complexes (38). Pre-edge transition areas, measured for C$_0$-CopA, M711A C$_2$-CopA, and C$_2$-CopA (dimensionless values of 0.557, 0.553, and 0.556, respectively) are also consistent with published values for three-coordinate Cu(I) model data. General edge features for all three samples were consistent with a partially asymmetric ligand coordination geometry slightly distored from trigional planar symmetry (38). EXAFS analyses are also consistent with three coordinate Cu(I)-nearest neighbor ligand environments; simulations indicate that the ligand sets are constructed by both sulfur and oxygen/nitrogen based ligands in all three samples. Raw EXAFS data with simulations along with their corresponding Fourier transforms are given for all three samples in Fig. 2. Fourier transforms for each show a dominant scattering contribution centered at a phase shifted bond length of ~1.8 Å (actual value of ~2.2 Å). Simulation results show a mixture of oxygen/nitrogen and sulfur ligation in the nearest neighbor environment for all samples, with M711A C$_2$-CopA having the highest ration of sulfur to oxygen/nitrogen ligation ratio (Table 3). In good agreement with the mutagenesis data, EXAFS simulations for the nearest neighbor environments in C$_0$-CopA (Site II occupied) indicate two disordered oxygen/nitrogen-based ligands at averaged bond lengths of ~2.03 Å, with an additional nearest neighbor sulfur ligand at a bond length of 2.31 Å. The relative ratio of oxygen/nitrogen *versus* sulfur ligation is reduced in the C$_2$-CopA spectral simulations, with a decrease in the copper-oxygen/nitrogen and copper-sulfur averaged bond length to 2.00 and 2.29 Å, respectively. Finally, fits to the M711A C$_2$-CopA (Site I occupied only) data showed an average copper-oxygen/nitrogen bond length at 2.04 Å with the highest relative percentage of copper-sulfur scattering in the three samples at an average bond length of 2.31 Å. High error bars in simulating
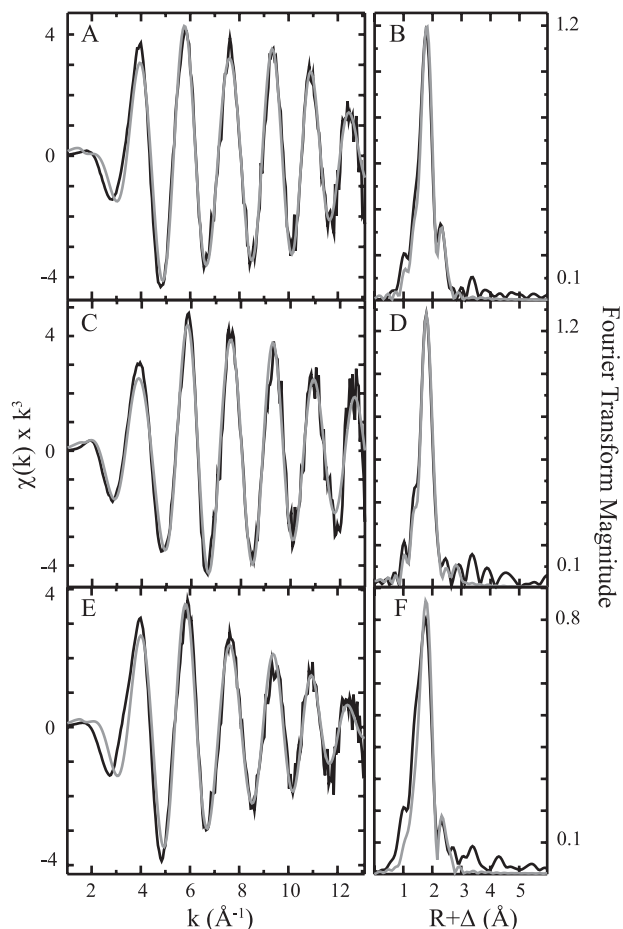
FIGURE 2. **CopA EXAFS data and simulations.** Raw EXAFS data for C$_0$-CopA (*A*), M^{711}A C$_2$-CopA (*C*), and C$_2$-CopA (*E*) in *black* with best fit simulated data in *green*. Phase shifted Fourier transforms of the protein copper data for C$_0$-CopA (*B*), M^{711}A C$_2$-CopA (*D*), and C$_2$-CopA (*F*) in *black* with simulated spectra in *gray*.

TABLE 3

Summary of averaged best fit parameters from the CopA copper EXAFS fitting analysis

The data are the averages of three independent data sets, fit over a *k* range of 1–12.85 Å^{-1}.

Sample	Ligand environment with oxygen, nitrogen, and sulfur scattering atoms[a]				Ligand Environment with carbon scattering atoms[a]				F′[f]
	Atom[b]	R[c]	C.N.[d]	s^{2} [e]	Atom[b]	R[c]	C.N.[d]	s^{2} [e,f]	
		Å				Å			
C$_0$-CopA	O/N	2.03	2.0	0.31	C	2.90	1.5	4.92	1.8
	S	2.31	1.0	1.80					
M^{711}A C$_2$-CopA	O/N	2.04	1.5	0.80	C	3.10	1.5	4.25	2.0
	S	2.31	1.5	3.67					
C$_2$-CopA	O/N	2.00	1.5	5.80	C	3.00	1.5	1.28	0.9
	S	2.29	1.0	3.10					

[a] Independent metal-ligand scattering environment.
[b] Scattering atoms: O (oxygen), N (nitrogen), S (sulfur), and C (carbon).
[c] Average metal-ligand bond length from three independent samples.
[d] Average metal-ligand coordination number (C.N.) from three independent samples.
[e] Average Debye-Waller factor in Å^2 × 10^3 from three independent samples.
[f] Number of degrees of freedom weighted mean square deviation between data and fit.

coordination numbers in EXAFS analysis ($\pm \sim 0.5$) make it impossible to obtain accurate values for this parameter; however, the tendency in the relative copper-oxygen/nitrogen *versus* sulfur coordination environments is consistent with the
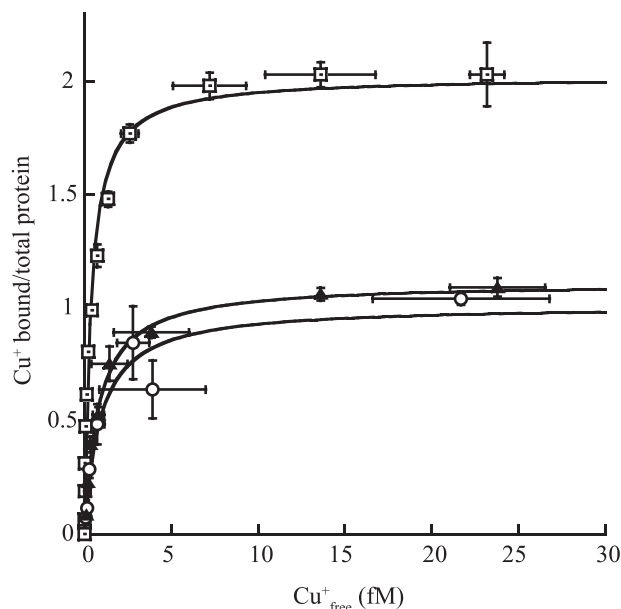

FIGURE 3. **K_a of transmembrane Cu$^+$ binding sites.** Cu$^+$ binding to C$_2$-CopA (site I and II functional), C382A C$_2$-CopA (Site II) and M711A C$_2$-CopA (Site I) was determined. The data were fitted using $n = 2.02 \pm 0.05$ and $K_a = 2.77 \pm 0.32$ fM^{-2} for C$_2$-CopA (□); $n = 1.01 \pm 0.06$ and $K_a = 1.12 \pm 0.25$ fM^{-1} for C$_0$-CopA (○) and $n = 1.11 \pm 0.05$ and $K_a = 1.30 \pm 0.22$ fM^{-1} for M711A C$_2$-CopA (▲). The values are the means $\pm$ S.E. ($n = 3$).

general trend expected moving from a Site II (Asn^{683}, Met^{711}, and Ser^{715}) to an average of Site I and II, to a complete Site I (Cys^{380}, Cys^{382}, and Tyr^{683}) ligand environment shifting from the C$_0$-CopA, to C$_2$-CopA, to M711A C$_2$-CopA samples. Finally, long range carbon scattering at $R > 2.9$ Å could be fit for all three samples. Carbon scattering at this distance typically arises from disordered scattering at a secondary position relative to the direct ligand atom.

Association Constants for the Equilibrium Cu$^+$ Binding to TM-MBS I and II—We have recently shown that the Cu$^+$-loaded chaperone, CopZ, delivers metal to CopA Cu$^+$ transmembrane sites (23). This vectorial Cu$^+$ exchange implies not only the specific interaction of both proteins but also the higher affinity of CopA sites for Cu$^+$. Testing this, the Cu$^+$ binding affinity of the TM-MBS was measured by means of competition with the Cu$^+$ indicator BCA (supplemental Fig. S2). A single apparent K_a was observable when both sites were present (C$_2$-CopA) (Fig. 3). As expected, this was higher (2-fold) than that observed under identical conditions for Cu$^+$ chaperone domain of *A. fulgidus* CopZ (23). By selectively mutating an amino acid in either site, we were able to determine the K_a of Site I (using the M711A C$_2$-CopA protein) or Site II (using C$_0$-CopA) (Fig. 3). In both cases K_a^{I} and K_a^{II} present a similar affinity for Cu$^+$. Moreover, determinations of Site II affinity using C382A or Y683A single mutants yielded similar values (2.6 ± 0.3 and 4.6 ± 0.8 fM^{-1}, respectively).

DISCUSSION

At the cross-roads of Cu$^+$ distribution and homeostasis mechanisms is its transport across membranes delimiting cellular compartments. Transmembrane proteins like the eukaryote Ctr proteins and the ubiquitous P$_{1B}$-type ATPases perform this task. The paramount event during this process is

Two Transmembrane Cu$^+$ Sites in Cu$^+$-ATPases

the ion binding to the transmembrane region of these proteins and subsequent translocation across the permeability barrier. Logically, the structure of the involved metal-binding sites determines the selectivity, kinetics, and energetics of transport. Here, we describe the transmembrane metal transport sites present in Cu$^+$-ATPases.

The Structure of Cu$^+$ Transport Sites—*A. fulgidus* CopA has two Cu$^+$-binding sites in its transmembrane region: Site I constituted by Cys[380], Cys[382], and Tyr[683] and Site II formed by Asn[683], Met[711], and Ser[715]. We previously reported that these are the only fully conserved amino acids observed in the transmembrane region of Cu$^+$-ATPases, and their mutation impairs Cu$^+$-dependent partial reaction in the ATPases catalytic cycle (22). Here, we show that these mutants are in fact unable to bind Cu$^+$ to transport sites. Furthermore, the combination of multiple mutations allowed pinpointing residues participating in each site. Further supporting the identity of these sites and the absence of adventitious sites generated in the mutants are the similar Cu$^+$ affinity constants observed in constructs where the sites are intact and in those carrying single site mutations.

This analysis should consider previous studies of yeast Cu$^+$-ATPase Ccc2, suggesting distinct roles for each transmembrane cysteine (45). It could be argued that this observation might be associated with the participation of each Cys in different metal sites. The authors hypothesized that the extremely slow phosphorylation of the C583S mutant suggests a distinct participation of this Cys in Cu$^+$ release. However, the apparent slow phosphorylation also observed in the D627A mutant (Asp[627] is the site of catalytic phosphorylation in Ccc2) points out the difficulties of working with a crude membrane system. On another hand, copper-independent phosphorylation by ATP of the wild type Thermotoga Cu$^+$-ATPase CopA has been demonstrated (46). Most important, because the copper dependence of the phosphorylation reaction or dephosphorylation rates was not explored in the Ccc2 mutants, conclusions on the roles of the transmembrane Cys on Cu$^+$ translocation are quite difficult to draw (45).

XAS studies corroborate the participation of sulfur and nitrogen/oxygen atoms and the trigonal coordination while they downplay a hypothetical involvement of additional side chains or backbone carbonyls in the metal coordination. Previously described Cu$^+$ sites have alternative functions and therefore appear as unfitting models for comparison with transport sites that transiently bind Cu$^+$. Nevertheless, the contrast of these sites reveals interesting aspects. For instance, Cu$^+$ coordination by Tyr, Ser, and Asn residues is rare. An analysis of close to 800 copper sites in proteins structures shows the well known coordination by Cys, His, and Met, but no Ser appear associated with copper binding and only a handful contains amino groups (Protein Data Bank entries 1jer and 1aqp) or coordinating Tyr (Protein Data Bank entries 1aqp, 1gof, and 1lcf). On the other hand, the presence of Cys and Met, the planar trigonal coordination, and the observed coordination distances are typical features of Cu$^+$ sites. Recently reported atomic models of Cu$^+$-ATPases based on electron crystallography data have suggested the structural proximity of helices H6, H7, and H8 (47, 48). Our mutagenesis and XAS results demonstrate the structural proximity and functional relation of these helices. However, adjustment of the described models taking into account XAS-derived distances was not possible. In fact, a forced displacement of the helices backbone would be required for modeling of Cu$^+$ TM-MBS into described P-type ATPase structures.

It is also relevant to emphasize the apparent independence of both sites. Although CopA binds two Cu$^+$ ions in the transmembrane region, these ions do not appear as di-metal copper centers. Distinctly, both sites can be independently loaded or removed; mutation of coordination residues in di-metal Cu centers appears to remove binding of both Cu ions (49). However, under *in vivo* conditions, where the chaperone delivers Cu$^+$ to these sites, they might not be independently functional. We think that Site I is likely to be facing the cytoplasmic entrance onto the ion path. Containing two Cys, Site I may be able to exchange Cu$^+$ with the corresponding Cu$^+$ chaperone. On the other hand, Site II containing Met[711] but no Cys is probably closer to the exiting (extracellular, luminal, or periplasmic) side of the membrane. In this direction, the preponderance of Met containing Cu$^+$ sites in periplasmic proteins has been reported (12–14). The short external loop between H7 and H8 is likely defined by highly conserved Pro in Cu$^+$-ATPases (Pro[688] and Pro[704] in CopA). Assuming a helical structure for these transmembrane segments, Met[711] and Asn[683] would be just 8–12 Å from the external loop in the aqueous medium. Although we have previously postulated a broad entrance into the cytoplasmic facing site (23, 32), the proximity of the Met to the external milieu suggests also a wide H$_2$O accessible channel reaching the extracellular facing site in a manner similar to that observed in the recently solved structures of Ca^{2+} and Na$^+$,K$^+$ ATPases (50, 51).

Mechanistic Implications—In the absence of other ligands, *A. fulgidus* CopA binds Cu$^+$ at the transport sites in a relatively irreversible form (very small k_{off}). This sets apart heavy metal ATPases (P$_{IB}$-type) from alkali metal ATPases (P$_{II}$-type). P$_{II}$-type ATPases need to undergo a conformational transition to occlude the transported cation and prevent backward release. Considering the physiological requirements of keeping Cu$^+$ in a bound form and the low affinity of CopA for the apo-form of the Cu$^+$ chaperone CopZ (23), the tight Cu$^+$ binding appears as a logic functional characteristic. Moreover, the enzyme has a metal affinity significantly larger than that of the chaperone. In the cell, this guarantees the vectorial metal transfer, although it certainly does not drive it. It might be considered that the Cu$^+$ TM-MBSs closely match those coordinating Ca^{2+} in the SERCA1 Ca^{2+}-ATPase. Thus, CopA Cys[382] and SERCA1 Glu[309] appear to share the same position in a disorganized helix open to the cytosol in the E1 conformation. Glu[309] appears located at the end of a "funnel" that directs Ca^{2+} to SERCA1 TM-MBS and is responsible for ion occlusion (52). Then, in the case of Cu$^+$-ATPases, it is tempting to speculate that the Cu$^+$-loaded chaperone follows a similar "funnel" where the transmembrane Cys might participate in Cu$^+$ transfer via a tricoordinated intermediary. On the other hand, although these findings explain significant aspects of Cu$^+$ transport by P-type ATPases and suggest interesting hypotheses, they also bring up challenging questions. For instance, how do these sites change upon enzyme phosphorylation such as their affinity being dramatically reduced, allowing Cu$^+$ release to the extracellular media?

Does the structure of the extracellular-facing access channel somewhat facilitate metal release or chelator access?

REFERENCES

1. Fraústro da Silva, J. J. R., and Williams, R. J. P. (2001) *The Biological Chemistry of the Elements*, 2nd Ed., pp. 418–435, Oxford Univesity Press, New York
2. Tapiero, H., Townsend, D. M., and Tew, K. D. (2003) *Biomed. Pharmacother.* **57,** 386–398
3. Lutsenko, S., LeShane, E. S., and Shinde, U. (2007) *Arch. Biochem. Biophys.* **463,** 134–148
4. Arnesano, F., Banci, L., Bertini, I., Ciofi-Baffoni, S., Molteni, E., Huffman, D. L., and O'Halloran, T. V. (2002) *Gen. Res.* **12,** 255–271
5. O'Halloran, T. V., and Culotta, V. C. (2000) *J. Biol. Chem.* **275,** 25057–25060
6. Rosenzweig, A. C., and Sazinsky, M. H. (2006) *Curr. Opin. Struct. Biol.* **16,** 729–735
7. MacPherson, I., and Murphy, M. (2007) *Cell Mol. Life Sci.* **64,** 2887–2899
8. Sakurai, T., and Kataoka, K. (2007) *Cell Mol. Life Sci.* **64,** 2642–2656
9. Ralle, M., Cooper, M. J., Lutsenko, S., and Blackburn, N. J. (1998) *J. Am. Chem. Soc.* **120,** 13525–13526
10. Pufahl, R. A., Singer, C. P., Peariso, K. L., Lin, S. J., Schmidt, P. J., Fahrni, C. J., Culotta, V. C., Penner-Hahn, J. E., and O'Halloran, T. V. (1997) *Science* **278,** 853–856
11. Liu, T., Ramesh, A., Ma, Z., Ward, S. K., Zhang, L., George, G. N., Talaat, A. M., Sacchettini, J. C., and Giedroc, D. P. (2007) *Nat. Chem. Biol.* **3,** 60–68
12. Bagai, I., Liu, W., Rensing, C., Blackburn, N. J., and McEvoy, M. M. (2007) *J. Biol. Chem.* **282,** 35695–35702
13. Loftin, I. R., Franke, S., Blackburn, N. J., and McEvoy, M. M. (2007) *Protein Sci.* **16,** 2287–2293
14. Xue, Y., Davis, A. V., Balakrishnan, G., Stasser, J. P., Staehlin, B. M., Focia, P., Spiro, T. G., Penner-Hahn, J. E., and O'Halloran, T. V. (2008) *Nat. Chem. Biol.* **4,** 107–109
15. Puig, S., Lee, J., Lau, M., and Thiele, D. J. (2002) *J. Biol. Chem.* **277,** 26021–26030
16. Aller, S. G., and Unger, V. M. (2006) *Proc. Natl. Acad. Sci. U. S. A.* **103,** 3627–3632
17. Eisses, J. F., and Kaplan, J. H. (2005) *J. Biol. Chem.* **280,** 37159–37168
18. Cox, D. W., and Moore, S. D. P. (2002) *J. Bioenerg. Biomembr.* **34,** 333–338
19. Lutsenko, S., Barnes, N. L., Bartee, M. Y., and Dmitriev, O. Y. (2007) *Phys. Rev.* **87,** 1011–1046
20. Axelsen, K. B., and Palmgren, M. G. (1998) *J. Mol. Evol.* **46,** 84–101
21. Argüello, J. M., Eren, E., and González-Guerrero, M. (2007) *Biometals* **20,** 233–248
22. Mandal, A. K., Yang, Y., Kertesz, T. M., and Argüello, J. M. (2004) *J. Biol. Chem.* **279,** 54802–54807
23. González-Guerrero, M., and Argüello, J. M. (2008) *Proc. Natl. Acad. Sci. U. S. A.* **105,** 5992–5997
24. Argüello, J. M. (2003) *J. Membr. Biol.* **195,** 93–108
25. Sazinsky, M. H., Agarwal, S., Argüello, J. M., and Rosenzweig, A. C. (2006) *Biochemistry* **45,** 9949–9955
26. Sazinsky, M. H., Mandal, A. K., Argüello, J. M., and Rosenzweig, A. C. (2006) *J. Biol. Chem.* **281,** 11161–11166
27. Dmitriev, O., Tsivkovskii, R., Abildgaard, F., Morgan, C. T., Markley, J. L., and Lutsenko, S. (2006) *Proc. Natl. Acad. Sci. U. S. A.* **103,** 5302–5307
28. Mandal, A. K., and Argüello, J. M. (2003) *Biochemistry* **42,** 11040–11047
29. Mandal, A. K., Cheung, W. D., and Argüello, J. M. (2002) *J. Biol. Chem.* **277,** 7201–7208
30. Eren, E., Kennedy, D. C., Maroney, M. J., and Argüello, J. M. (2006) *J. Biol. Chem.* **281,** 33881–33891
31. Bradford, M. M. (1976) *Anal. Biochem.* **72,** 248–254
32. Yang, Y., Mandal, A. K., Bredestón, L. M., Luis González-Flecha, F., and Argüello, J. M. (2007) *Biochim. Biophys. Act.* **1768,** 495–501
33. Brenner, A. J., and Harris, E. D. (1995) *Anal. Biochem.* **226,** 80–84
34. Yatsunyk, L. A., and Rosenzweig, A. C. (2007) *J. Biol. Chem.* **282,** 8622–8631
35. Deleted in proof
36. Ankudinov, A. L., and Rehr, J. J. (1997) *Phys. Rev.* **B56,** R1712–R1715
37. Lieberman, R. L., Kondapalli, K. C., Shrestha, D. B., Hakemian, A. S., Smith, S. M., Telser, J., Kuzelka, J., Gupta, R., Borovik, A. S., Lippard, S. J., Hoffman, B. M., Rosenzweig, A. C., and Stemmler, T. L. (2006) *Inorg. Chem.* **45,** 8372–8381
38. Kau, L. S., Spira-Solomon, D. J., Penner-Hahn, J. E., Hodgson, K. O., and Solomon, E. I. (1987) *J. Am. Chem. Soc.* **109,** 6433–6442
39. Cattoni, D. I., González-Flecha, F. L., and Argüello, J. M. (2008) *Arch. Biochem. Biophys.* **471,** 198–206
40. Missiaen, L., Wuytack, F., De Smedt, H., Vrolix, M., and Casteels, R. (1988) *Biochem. J.* **253,** 827–833
41. Glynn, I. M., and Richards, D. E. (1982) *J. Physiol.* **330,** 17–43
42. Moreira, O. C., Ríos, P. F., and Barrabin, H. (2005) *Biochim. Biophys. Acta* **1708,** 411–419
43. Esman, M., and Skou, J. C. (1985) *Biochem. Biophys. Res. Commun.* **127,** 857–863
44. Fujimori, T., and Jencks, W. P. (1990) *J. Biol. Chem.* **265,** 16262–16270
45. Lowe, J., Vieyra, A., Catty, P., Guillain, F., Mintz, E., and Cuillel, M. (2004) *J. Biol. Chem.* **279,** 25986–25994
46. Hatori, Y., Hirata, A., Toyoshima, C., Lewis, D., Pilankatta, R., and Inesi, G. (2008) *J. Biol. Chem.* **283,** 22541–22549
47. Chintalapati, S., Al Kurdi, R., van Scheltinga, A. C. T., and Kühlbrandt, W. (2008) *J. Mol. Biol.* **378,** 581–595
48. Wu, C. C., Rice, W. J., and Stokes, D. L. (2008) *Structure* **16,** 976–985
49. Pritz, R. A., Ho, L., Furumura, M., and Hearing, V. J. (1997) *J. Investig. Dermatol.* **109,** 207–212
50. Olesen, C., Picard, M., Winther, A.-M. L., Gyrup, C., Morth, J. P., Oxvig, C., Moller, J. V., and Nissen, P. (2007) *Nature* **450,** 1036–1042
51. Morth, J. P., Pedersen, B. P., Toustrup-Jensen, M. S., Sorensen, T. L. M., Petersen, J., Andersen, J. P., Vilsen, B., and Nissen, P. (2007) *Nature* **450,** 1043–1049
52. Toyoshima, C., and Inesi, G. (2004) *Annu. Rev. Biochem.* **73,** 269–292